UDK 539.383:669.1:355.691.2
Original scientific article/Izvirni znanstveni članek

ISSN 1580-2949
MTAEC9, 56(2)87(2022)

HOT-COMPRESSION DEFORMATION BEHAVIOR AND CONSTITUTIVE EQUATIONS OF LZ50 AXLE STEEL

OBNAŠANJE JEKLA ZA OSI VRSTE LZ50 MED VROČO TLAČNO DEFORMACIJO IN NJENE KONSTITUTIVNE ENAČBE

Dong-sheng Jia[1], Tao He[1*], Yuan-ming Huo[1], Xiang-yang Du[1], Bao-yu Wang[2], Shi-qian Li[1], Han-lin Li[1]

[1]School of Mechanical and Automotive Engineering, Shanghai University of Engineering Science, Shanghai 101600, China
[2]School of Mechanical Engineering, University of Science and Technology Beijing, Beijing 100083, China

Prejem rokopisa – received: 2021-12-09; sprejem za objavo – accepted for publication: 2022-01-17

doi:10.17222/mit.2021.331

A study of deformation behavior of LZ50 axle steel has great significance to the railway industry. Hot-deformation tests were performed using a Gleeble-3800 thermal mechanical simulator at temperatures of (900, 1000 and 1100) °C with strain rates of (0.1, 1.0 and 10.0) s^{-1} under different deformation degrees of 0.2, 0.6 and 1.0. True stress-strain curves were discussed to obtain hot-processing maps. Then hot-processing maps of LZ50 steel at different deformation parameters were discussed including safe zones and unsafe zones. Finally, thermal deformation constitutive equations and dynamic recrystallization models were established based on the experimental data. The results show that at a strain rate of 10.0 s^{-1}, the peak value of the flow stress increases by approximately 40 MPa with a decrease in the temperature from 1000 °C 900 °C, which is larger than the value of 18 MPa obtained at a decrease from 1100 °C to 1000 °C. At deformation temperatures of 900–1000 °C, the peak value of the flow stress increases by approximately 37 MPa with the strain rate increasing from 0.1 s^{-1} to 1.0 s^{-1}, while from 1.0 s^{-1} to 10.0 s^{-1}, the increase is approximately 21 MPa. With an increase in the strain from 0.2 to 1.0, the instability area under the low deformation temperature expands due to a higher strain rate. The activation energy of dynamic recrystallization is 334.537 kJ/mol.

Key words: LZ50 axle steel, hot compression, thermal deformation, constitutive equation, dynamic recrystallization, processing map

Študij deformacije jekla za osi vrste LZ50 je zelo pomemben za industrijo železniškega transporta. Avtorji članka so izvajali vroče teste tlačne deformacije na termo-mehanskem simulatorju Gleeble-3800 pri temperaturah (900, 1000 in 1100) °C ter hitrostih deformacije (0,1, 1,0 in 10,0) s^{-1} in z različno stopnjo deformacije 0,2, 0,6 in 1,0. V pričujočem članku razpravljajo o dobljenih krivuljah resnična napetost-resnična deformacija, potrebnih za izdelavo vročih procesnih map in nato opisujejo le-te za jeklo LZ50 glede na različne deformacijske parametre, vključno z obravnavanjem varnih in nevarnih področij oziroma območij. Na koncu so na osnovi eksperimentalnih podatkov izdelali še termične deformacijske konstitutivne enačbe in modele dinamične rekristalizacije. Rezultati analiz kažejo, da maksimalna vrednost napetosti tečenja pri hitrosti deformacije 10 s^{-1} naraste za približno 40 MPa pri znižanju temperature s 1000 °C na 900 °C, kar je 18 MPa oziroma več kot pri znižanju temperature s 1100 °C na 1000 °C. Pri deformacijskih temperaturah 900 °C ali 1000 °C maksimalna vrednost napetosti tečenja naraste za približno 37 MPa pri povečanju hitrosti deformacije z 0,1 s^{-1} na 1 s^{-1}, medtem ko je prirastek napetosti tečenja približno 21 MPa pri povečanju hitrosti deformacije z 1 s^{-1} na 10 s^{-1}. S povečanjem deformacije z vrednosti 0,2 na 1,0 se področje nestabilnosti nizke temperature deformacije razširi k višjim hitrostim deformacije. Ugotovili so, da je aktivacijska energija za dinamično rekristalizacijo enaka približno 335 kJ/mol.

Ključne besede: jeklo za osi vrste LZ50, vroča tlačna deformacija, termična deformacija, konstitutivne enečbe, dinamična rekristalizacija, procesna mapa

1 INTRODUCTION

Mechanical properties of materials vary under the influence of different microstructures. In hot deformation, microstructure evolution including strain hardening, recovery, recrystallization and grain growth takes place and the forms of microstructures are closely associated with thermomechanical parameters such as strain, strain rates, temperature and initial microstructure of materials.[1] Meanwhile, the values of the flow stress, working forces and stored energy presented at the end of deformation are determined by these parameters that are of great significance for designers to develop a suitable metal-forming processing technology.[2] Otherwise, high-temperature plastic constitutive equations and hot-processing maps can be established using thermomechanical parameters and the value of the flow stress used to determine the loading value and energy consumption in reality. These equations and maps can not only reflect the relationships between thermomechanical parameters used for numerical simulation but also show the safety zones during processing to avoid the occurrence of defects.[3] As one of the most important parts, the axle plays an irreplaceable role in bearing the weight and complex stress of a train. Higher mechanical properties of the axle steel are required because of the development of high-speed and heavy-haul railways. Two steps that can change the mechanical properties of axles during

*Corresponding author's e-mail:
hetao@sues.edu.cn

Table 1: Chemical composition of LZ50 steel (*w*/%)

C	Mn	Si	P	S	Cr	Ni	Cu	Al	V	N	Fe
0.51	0.74	0.29	0.008	0.002	0.013	0.008	0.006	0.006	0.02	0.0034	bal.

processing are forging and heat treatment. In this study, hot-compression tests are performed to replace forging and find the best process parameters for the LZ50 axle steel, which is one of the widely applied axle materials in the railway-manufacturing industry due to its good mechanical properties under extreme conditions.[4,5]

Numerous researchers focused on hot-compressive deformation behavior and microstructure-evolution rules of axle steels during hot forming, but few of them focused on LZ50 steel. Huo et al.[6] investigated the deformation behaviors and microstructure evolution of 25CrMo4 at temperatures of 1040–1160 °C and strain rates of 1.0–10.0 s^{-1} under different deformation degrees from 0 to 0.8 using a Gleeble thermal mechanical simulator. Zhang et al.[7] obtained the flow-stress constitutive equation of DZ2 steel by thermal mechanical testing and established processing maps under different strain rates. Du et al.[8] studied the hot-deformation and dynamic-recrystallization behaviors of LZ50 steel in the temperature range of 870–1170 °C at strain rates of 0.05–3 s^{-1}, and then developed the flow-stress constitutive equation and kinetic equation. Zheng et al.[9] obtained the plastic constitutive equation of LZ50 steel at high temperature and analyzed its dynamic-recrystallization behaviors under different thermal-deformation conditions.

Therefore, more research is necessary to investigate the hot-deformation behaviors of LZ50 steel. Optimized parameters can be used to obtain better mechanical properties for practical work. In this study, hot-compression tests are processed at different temperatures, different deformation degrees as well as different strain rates. Then, the test results are analyzed to obtain flow-stress curves, hot-processing maps, high-temperature plastic constitutive equations and dynamic-recrystallization models. Finally, the effects of the processing parameters on hot-deformation behaviors are discussed.

2 EXPERIMENTAL PART

The chemical composition of the LZ50 experimental material, which belongs to medium-carbon high-strength carbon steel, is shown in **Table 1**. The temperatures of A_{c1} and A_{c3} for this steel were 725 °C and 760 °C, respectively. Original samples were machined into cylindrical compression specimens of 8 mm in diameter and 15 mm in length with a lathe to obtain the target surface roughness, as shown in **Figure 1**. Then, the specimens were tested using a Gleeble-3800 thermal mechanical simulator to obtain the stress-strain curves. **Figure 2** illustrates the experimental programme for the hot-compression test. The specimens were heated to (900, 1000 and 1100) °C at a heating rate of 5 °C/s. Then, each specimen was soaked at its own final temperature for 3 min to achieve complete austenitization. Hot-compression experiments were conducted at strain rates of (0.1, 1.0 and 10) s^{-1}. The specimens were compressed to one of the following true strains: 0.2, 0.6 or 1.0. After the compression, the specimens were quenched using water cooling immediately to retain the microstructure.

Compressed specimens with different "dump-type" figures caused by different true strains are shown in **Fig-**

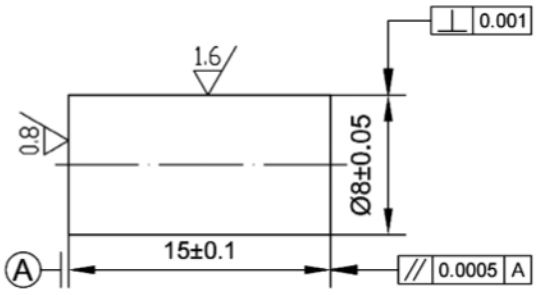

Figure 1: Dimensions of compression specimens (mm)

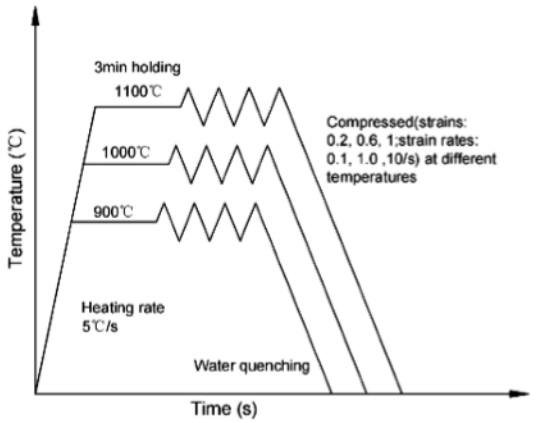

Figure 2: Experimental processes

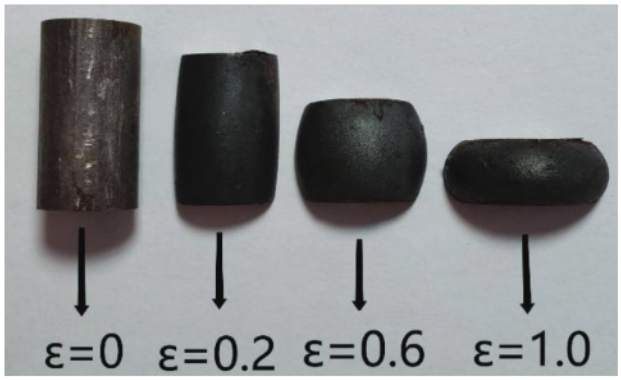

Figure 3: Sample morphology at different strain levels after compression

ure 3. Their stress-strain curves were measured using the C-gauge thermal mechanical simulator.

3 RESULTS AND DISCUSSION

3.1 Hot-compression behavior of LZ50 axle steel

Figure 4 shows the true stress-strain curves at different deformation temperatures and strain rates of (0.1, 1.0 and 10.0) s^{-1}. With the increasing strain rate, an increase in the peak value of the flow stress is obvious. For example, at the strain rate of 1.0 s^{-1} and the temperature of 1000–900 °C, the peak stress is increased by 16.7 %, while in the range of 1100–1000 °C and at the strain rate of 10.0 s^{-1}, it is increased by 122.2 %.

Figure 5 shows the true stress-strain curves under different strain rates and different forming temperatures of (900, 1000 and 1100) °C. The peak value of the flow stress increases with the increasing strain rate. At the deformation temperature of 900 °C, the peak value of the flow stress increases by approximately 37 MPa with the strain rate increasing from 0.1 s^{-1} to 1.0 s^{-1}. At the same temperature, the increase is approximately 21 MPa from 1.0 s^{-1} to 10.0 s^{-1}, which is lower than 37 MPa. Similarly, this phenomenon occurs at other deformation temperatures. Otherwise, at 900 °C, the inflection point of the peak value is obvious under the strain rate of 0.1 s^{-1}. However, the curves gradually become flat with increasing strain rates.

There are three stages of microstructure evolution during hot compression: work hardening, dynamic recovery and dynamic recrystallization. As shown in **Figure 6**, the curve of dynamic recrystallization illustrates tendencies of increasing, decreasing and finally flattening. This is because at the beginning of deformation, the value of work hardening triggered by a dislocation increment is larger than the value of dynamic softening caused by dislocation climbing and cross slip.[10] The flow stress rises gradually with the increasing deformation degree, dislocation accumulation and thermal activation energy aggregation. When it reaches the critical strain, there is enough activation energy to introduce dynamic recrystallization so that the dynamic softening is larger than work hardening and the curve declines. As the deformation degree continues to increase, the activation energy decreases until the value of work hardening is equal to the value of dynamic softening. At this moment, the curve begins to flatten.

As shown in **Figure 4**, the peak value of the flow stress decreases with the increasing forming temperature and decreasing strain rate. This is because higher temperatures lead to faster aggregation rates of the thermal activation energy, which can eliminate dislocations within the cells. Then, the value of work hardening is equal to the value of previous dynamic softening. However, the influence of the strain rate on work hardening cannot be ignored: lower strain rates ensure a sufficient incubation time for the dynamic-recrystallization behavior to form new grains around old grains.[11] Therefore, the curves of dynamic recrystallization are not obvious with the increasing strain rates. Under the effect of a higher strain rate, the peak value of the flow stress is higher

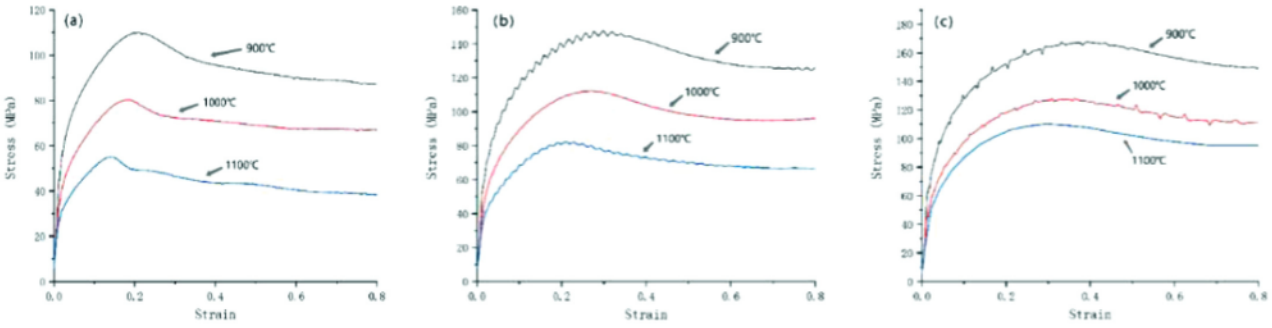

Figure 4: Hot-compression deformation behavior of LZ50 steel at: a) strain rate of 0.1 s^{-1}, b) strain rate of 1.0 s^{-1}, c) strain rate of 10.0 s^{-1}

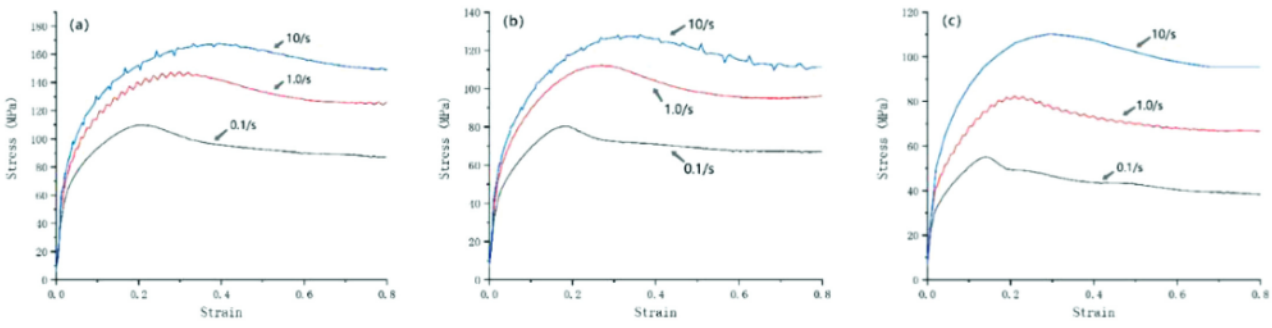

Figure 5: Hot-compression deformation behavior of LZ50 steel at forming temperatures of: a) 900 °C, b) 1000 °C, c) 1100 °C

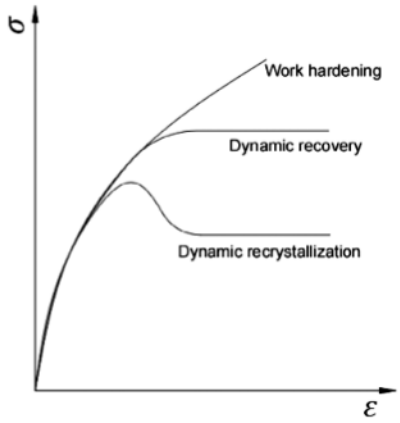

Figure 6: Relationship between the flow stress and microstructure during hot working

than that of a lower strain rate, which can be seen in **Figure 5**.

3.2 Establishment of a hot-processing map

A hot-processing map is a figure that can evaluate the processability of a material. It can be used to analyze and predict deformation characteristics or deformation mechanisms of a material under different forming conditions. This data is processed to obtain the safe zones and unsafe zones of hot-deformation activities to avoid an occurrence of defects. They can also be used to optimize the processing parameters for good microstructures.

Two models are suitable for the construction of thermal-processing maps. One is named the atomic model, used to establish a Raj processing map, while the other map is based on the dynamic material model.[12] The Raj[13] processing map has usage restrictions in actual applications because it has to solve a large number of parameters and can only be used under steady state conditions. Therefore, the map based on the dynamic material model proposed by Prasad[14] is widely used. Prasad believed that the processing of materials can be seen as an energy-dissipation system. Part of the energy is consumed during the plastic deformation of the material and converted into heat. The remaining energy is used to promote the evolution of the microstructure. The Equations (1) to (4) proposed by Prasad are shown below:

$$P = \sigma \cdot \dot{\varepsilon} = G + J \tag{1}$$

$$m = \frac{\partial J}{\partial G} = \frac{\partial \log \sigma}{\partial \log \dot{\varepsilon}} \tag{2}$$

$$\eta = \frac{J}{J_{\max}} = \frac{2m}{m+1} \tag{3}$$

$$\xi(\dot{\varepsilon}) = \frac{\partial \log\left(\frac{m}{m+1}\right)}{\partial \log \dot{\varepsilon}} + m \tag{4}$$

where P is the energy absorbed per unit volume of the material during processing, G is the dissipator content, J is the dissipator co-content, m is the strain rate sensitivity index, η is the efficiency of dissipation and $\xi(\dot{\varepsilon})$ is the instability factor. When it is lower than 0, the area is found to be an instability area.

To ensure the reliability of hot-processing maps, the thermal-compression test data was expanded using the cubic-spline interpolation method shown in **Table 2**. Then the values of m, η and ξ were calculated to draft the power-dissipation efficiency map and instability map. Finally, hot-processing maps shown in **Figure 7** were formed by superimposing two maps. In **Figure 7**, the values on the isoline are η. The shaded areas indicate the instability zones.

Table 2: Values of stress at different deformation conditions

σ/MPa	T/°C	$\dot{\varepsilon}$/s^{-1}		
		0.1	1	10
ε = 0.2	900	111.77	113.59	129.54
	1000	76.86	94.95	100.04
	1100	59.45	72.66	72.85
ε = 0.6	900	113.25	115.12	182.67
	1000	79.98	113.58	126.6
	1100	54.92	78.76	97.96
ε = 1.0	900	109.9	147.81	167.86
	1000	80.24	112.29	128.25
	1100	55.04	82.46	110.27

As shown in **Figure 7**, the instability zone expands with the increasing strain. The value of the efficiency of dissipation η increases with increasing deformation temperature and decreasing strain rate. Different values of η

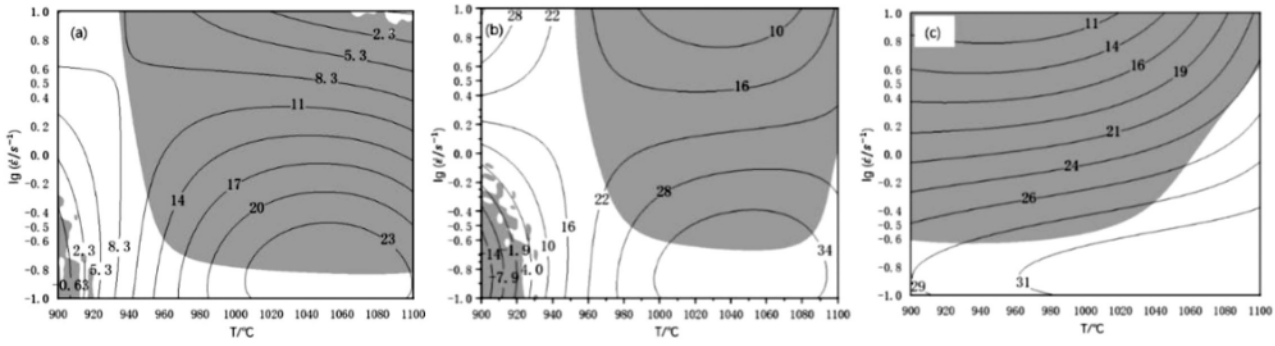

Figure 7: Processing maps of LZ50 steel at different true strains: a) ε = 0.2, b) ε = 0.6, c) ε = 1.0

reflect different mechanisms of microstructure evolution. A higher value of η indicates a higher chance of recrystallization because of its sufficient energy and incubation time. With the increase in the strain from 0.2 to 1.0, the instability area under low deformation temperatures from 900–940 °C expands due to a higher strain rate. Meanwhile, the instability area under high deformation temperatures from 1000–1100 °C decreases because of its softening effect.

Figure 7a shows the condition of the deformation degree of 0.2. Whether at high or low temperatures, safe zones are always distributed in the areas with lower strain rates. Low deformation cannot provide sufficient incubation time to soften the materials. In this case, increasing the strain rate can easily cause damage and cracking of the materials. With the increase in the true strain shown in **Figures 7b** and **7c**, the enhancement of the softening effect expands the strain rate range when the material is deformed. However, this phenomenon does not apply to low-temperature areas where the work hardening effect is greater than the softening effect.

3.3 Establishment of constitutive equations

3.3.1 Thermal-deformation constitutive equation

Thermal-deformation constitutive equations reflect the relationships between the flow stress, strain rate and forming temperature, which are helpful for numerical simulation. An equation can be represented using the hyperbolic-sine law proposed by Sellars and Tegart,[15] as shown in Equation (5):

$$\dot{\varepsilon} = A[\sinh(\alpha\sigma)]^n \exp\left(-\frac{Q}{RT}\right) \tag{5}$$

where A is the material parameter, α is the stress-level parameter (mm^2/N), σ is the flow stress (MPa), n is the stress index, Q is the hot-deformation activation energy (kJ/mol), T is the absolute temperature (K), and R is the universal gas constant (8.3145 J/(mol·K)).

According to the level of the flow stress of the metal material, the relationship shown in Equation (5) can be simplified as follows:

$$\dot{\varepsilon} = \begin{cases} A_1 \sigma^{n_1} \exp\left(-\dfrac{Q}{RT}\right) & , \alpha\sigma < 0.8 \quad (6) \\ A_2 \exp(\beta\sigma) \exp\left(-\dfrac{Q}{RT}\right), & \alpha\sigma > 1.2 \quad (7) \end{cases}$$

where A_1, A_2, n_1, β are material parameters and $\alpha = \beta/n_1$. Meanwhile, the Zener-Hollomon parameter shown in Equation (8) is needed to describe the relationship between the strain rate and deformation temperature:

$$Z = \dot{\varepsilon} \exp\left(\frac{Q}{RT}\right) \tag{8}$$

where Z is the strain-rate factor of temperature compensation. Then Equations (9) and (10) are proposed, taking the logarithms of Equations (5) to (7), respectively.

$$\ln\dot{\varepsilon} = \ln A - \frac{Q}{RT} + n \ln[\sinh(\alpha\sigma)] \tag{9}$$

$$\ln\dot{\varepsilon} = n_1 \ln\sigma + \ln A_1 - \frac{Q}{RT} \tag{10}$$

$$\ln\dot{\varepsilon} = \beta\sigma + \ln A_2 - \frac{Q}{RT} \tag{11}$$

3.3.1.1 Solution for the activation energy of dynamic recrystallization

Equations (5) to (7) show that the relationships between $\ln\dot{\varepsilon}$ and $\ln[\sinh(\alpha\sigma)]$, $\ln\sigma$ or σ are linear at certain temperatures. This means that $n_1 = d\ln\dot{\varepsilon}/d\ln\sigma$, $\beta = d\ln\dot{\varepsilon}/d\sigma$, $n = d\ln\dot{\varepsilon}/d\ln[\sinh(\alpha\sigma)]$. The pictures of $\ln\dot{\varepsilon}$–$\ln\sigma$ and $\ln\dot{\varepsilon}$–σ (shown in **Figure 8**) were drafted using the data from hot-compression tests with a deformation degree of 1.0. Then, the values of $n_1 = 8.78$ and $\beta = 0.2526$ can be calculated taking the average of the slope of each set of fitted lines in the figures. The value of $\alpha = 0.0287699$ can be calculated by putting n_1 and β into the equation $\alpha = \beta/n_1$. The picture of $\ln\dot{\varepsilon}$–$\ln[\sinh(\alpha\sigma)]$ was presented in the same way. The value of $n = 2.8923$ was calculated using the average value of the slope of the fitted lines shown in **Figure 9**. According to Equation (5), the value of

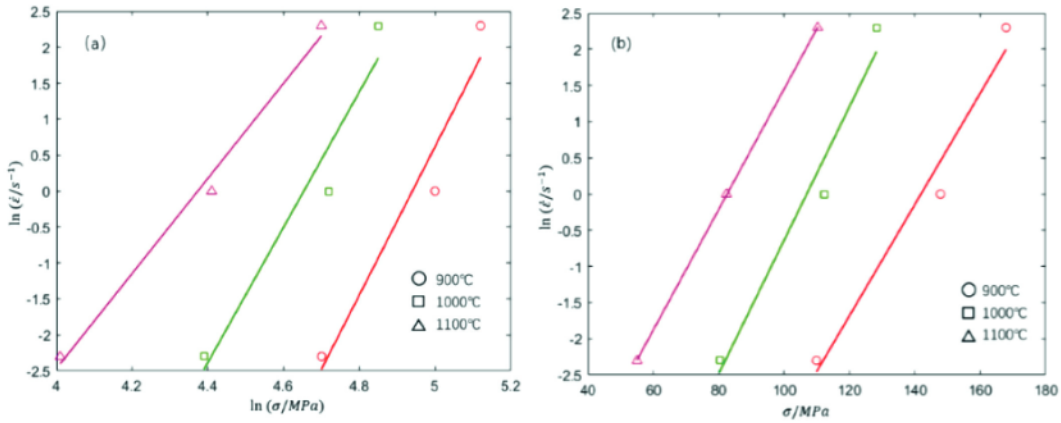

Figure 8: Relationship between: a) $\ln\dot{\varepsilon}$–$\ln\sigma$ and b) $\ln\dot{\varepsilon}$–σ

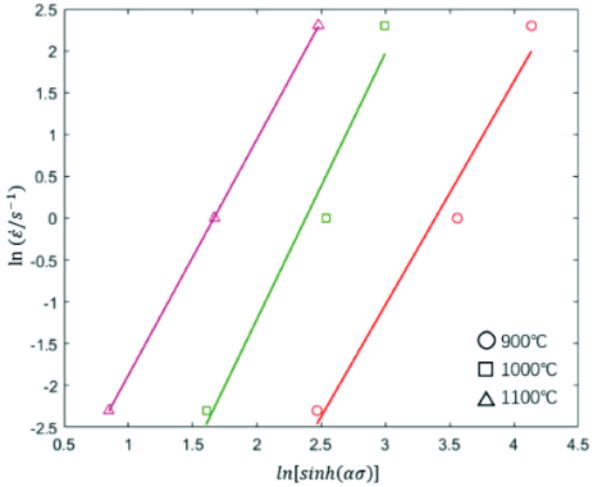

Figure 9: Relationship between lnε̇ and ln[sinh(ασ)]

$K = Q/(n \cdot R) = 13.9112$ can be calculated with the picture of ln[sinh(ασ)]–1000/T shown in **Figure 10**. Then the value of the activation energy of dynamic recrystallization was presented: $Q = K \cdot n \cdot R = 334.537$ kJ/mol. Finally, Equation (12) was proposed using the value of Q:

$$Z = \dot{\varepsilon} \exp\left(\frac{334537}{8.3145 \times T}\right) \tag{12}$$

3.3.1.2 Establishment of the flow-stress constitutive equation

Equation (13) is proposed taking the logarithm of Equation (4). In addition, Equation (14) is equal to Equation (9) because of the properties of the hyperbolic-sine law. After the calculation, Equation (15) is presented as follows:

$$\ln Z = \ln A + n \ln[\sinh(\alpha\sigma)] \tag{13}$$

$$\left(\frac{Z}{A}\right)^{\frac{1}{n}} = \sinh(\alpha\sigma) = \frac{\varepsilon^{\alpha\sigma} - e^{-\alpha\sigma}}{2} \tag{14}$$

$$\sigma = \frac{1}{\alpha} \ln\left\{\left(\frac{Z}{A}\right)^{\frac{1}{n}} + \left[\left(\frac{Z}{A}\right)^{\frac{2}{n}} + 1\right]^{\frac{1}{2}}\right\} \tag{15}$$

It is obvious that the relationship of ln$Z$ and ln[sinh(ασ)] is linear. The picture of ln$Z$–ln[sinh(ασ)] was drafted to obtain the mean value of the intercept of the fitted lines shown in **Figure 11**. Then the value of A was calculated as 4.9079×10^{10}. Finally, putting all the calculated parameters into Equations (1) and (11), the relationship between the strain rate, flow stress and forming temperature, and the flow-stress constitutive equation of LZ50 steel are shown in Equations (16) and (17), respectively.

$$\dot{\varepsilon} = 4.9079 \cdot 10^{10} [\sinh(0.0287699\sigma)]^{2.8923} \cdot \cdot \exp\left(\frac{334537}{8.3145 \times T}\right) \tag{16}$$

$$\sigma = \frac{1}{0.0287699}\left\{\left(\frac{Z}{4.9079 \cdot 10^{10}}\right)^{\frac{1}{2.8923}} + \left[\left(\frac{Z}{4.9079 \cdot 10^{10}}\right)^{\frac{2}{2.8923}} + 1\right]\right\} \tag{17}$$

where $Z = \dot{\varepsilon} \cdot \exp(334537/8.3145T)$.

To verify the accuracy of the constitutive equation, **Table 3** shows a comparison of the calculated and experimental values at different temperatures and different strain rates under a deformation degree of 1.0. By comparison, it can be seen that the values of the calculation are very close to the values of the experiment. The maximum relative error is 5.84 %, and the absolute value of

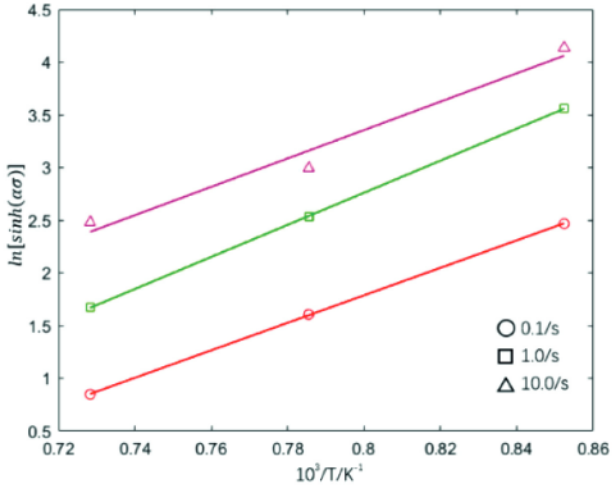

Figure 10: Relationship between ln[sinh(ασ)] and 1000/T

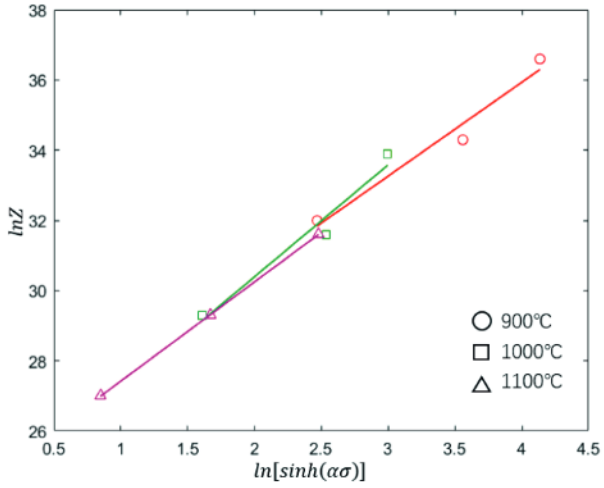

Figure 11: Relationship between ln$Z$ and ln[sinh(ασ)]

the average relative error is only 2.60 %. Therefore, the equation is accurately enough to provide a theoretical basis for the actual hot forming of LZ50 axle steel.

Table 3: Comparison of theoretical and experimental results of the peak stress (MPa)

strain rate (s^{-1})	experimental result	theoretic result	relative error
900 °C			
0.1	109.90	112.81	2.65 %
1	147.81	140.44	–4.99 %
10	167.86	168.10	0.14 %
1000 °C			
0.1	80.24	80.72	0.60 %
1	112.29	108.12	–3.71 %
10	128.25	135.74	5.84 %
1100 °C			
0.1	55.04	54.29	–1.36 %
1	82.46	80.73	–2.10 %
10	110.27	108.13	–1.94 %

3.3.2 Dynamic recrystallization models

In general, the thermodynamic conditions of DRV and DRX are prepared at the beginning of hot deformation because their driving force is activation energy, which can be stored under any slight deformation. However, the nucleation process of DRX (including nucleation and grain growth) is presented in the areas with great strain hardening. Therefore, another prerequisite of DRX is the critical deformation degree marked as ε_c. With the increasing forming degree, the effect of DRX gradually increases. Finally, the value of the flow stress attains its peak when the effect of DRX is equal to that of strain hardening. The value of the strain under the peak flow stress is known as the peak strain, marked as ε_p. The work above shows that the level of DRX is related to the strain rate, forming temperature and deformation degree. Then these different deformation parameters lead to different microstructures, which have an important effect on the material performance. Therefore, it is necessary to establish dynamic-recrystallization models for predicting and controlling the microstructure evolution.

3.3.2.1 DRX model of the critical strain

With the increasing true strain, dislocations continue to accumulate, inducing an increase in the work-hardening rate $\theta(\mathrm{d}\theta/\mathrm{d}\varepsilon)$. When the true strain reaches the critical strain, the behavior of dynamic softening including dynamic recovery and dynamic recrystallization, is stimulated to resist the work hardening. Therefore, the work-hardening rate shows the following trends: it increases first and then declines to a negative number (the zero point is called the peak strain ε_p), then it increases to zero again, remaining at the zero point (at the strain of steady-state dynamic recrystallization ε_{ss}). To find the values of ε_p and ε_{ss}, **Figure 12a** was drafted using the experimental data.

Sellars[16] found the relationship between ε_c and ε_p shown in Equations (18) and (19). Then Equation (20) was proposed by taking the logarithm of Equation (19):

$$\varepsilon_c = a\varepsilon_p \tag{18}$$

$$\varepsilon_p = kZ^q \tag{19}$$

$$\ln \varepsilon_p = \ln k + q \ln Z \tag{20}$$

where ε_c is the critical strain of DRX, ε_p is the peak value of the strain of DRX and a, k and q are material constants. In accordance with the work described in section 3.3.1 of this paper, the relationship of Z, T and $\dot{\varepsilon}$ is shown in Equation (12). The $\ln\varepsilon_p$–$\ln Z$ curves under different conditions were drafted as shown in **Figure 13**. The values of q = 0.1443 and k = 0.00263 were calculated taking the average of the slopes of the lines. The value of a = 0.5146 was obtained through the experiments performed by Du.[8] Finally, the DRX model of the critical strain and peak strain are presented as follows:

$$\varepsilon_c = 0.5146\varepsilon_p \tag{21}$$

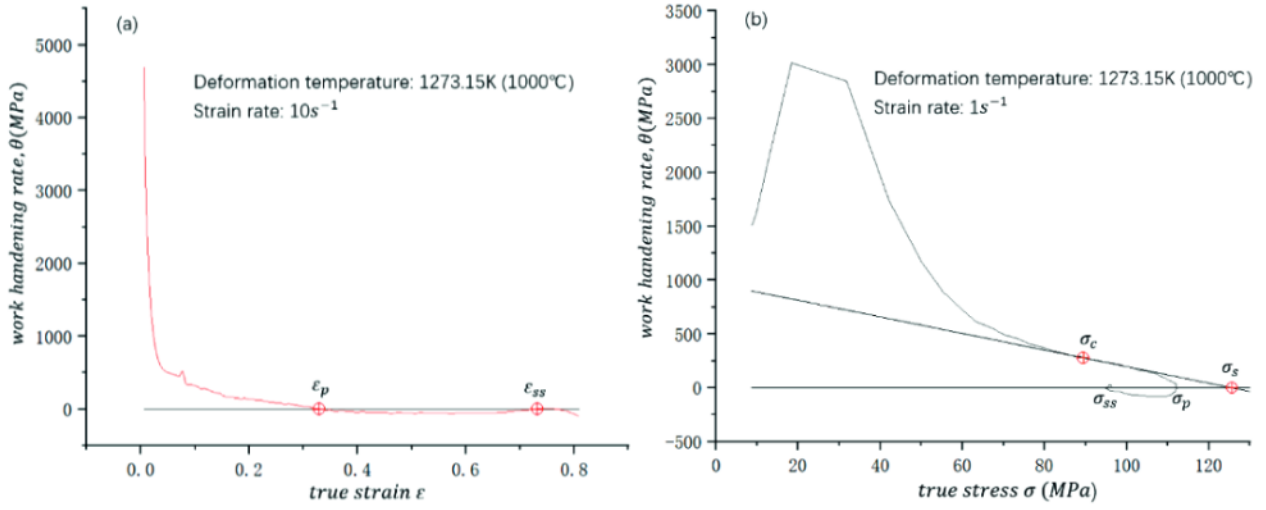

Figure 12: Relationship at 1273.15 K (1000 °C) between: a) θ and ε with a strain rate of 10 s^{-1} and b) θ and σ with a strain rate of 1.0 s^{-1}

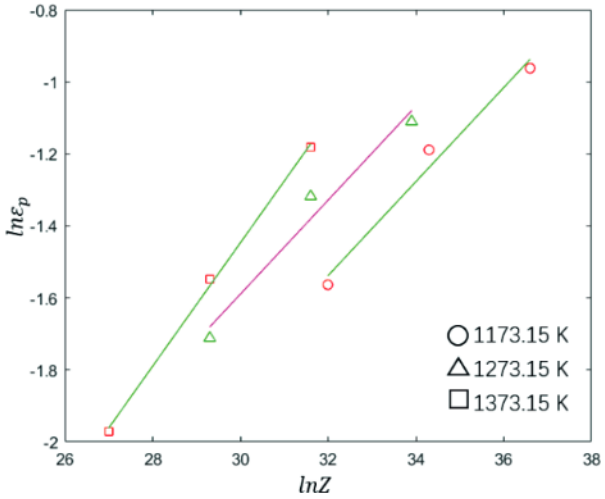

Figure 13: Relationship between peak strain ε_p and Z under different deformation temperatures

$$\varepsilon_p = 0.00263Z^{0.1443} \quad (22)$$

3.3.2.2 Kinetic model of DRX

The Avrami equation is used to describe the relation between the fraction of dynamic recrystallization (X_{drex}) and strains:[17]

$$X_{drex} = 1 - \exp\left[-\beta_d \left(\frac{\varepsilon - \varepsilon_c}{\varepsilon_p}\right)^{k_d}\right] \quad (23)$$

$$\ln\left[-\ln(1 - X_{drex})\right] = \ln\beta_d + k_d \ln\left(\frac{\varepsilon - \varepsilon_c}{\varepsilon_p}\right) \quad (24)$$

where β_d and k_d are the influencing factors of dynamic recrystallization. To determine the value of the dynamic-recrystallization volume fraction, Equation (25) was proposed as follows:[18,19]

$$X_{drex} = \frac{\sigma_{recov} - \sigma_{drx}}{\sigma_s - \sigma_{ss}} \quad (25)$$

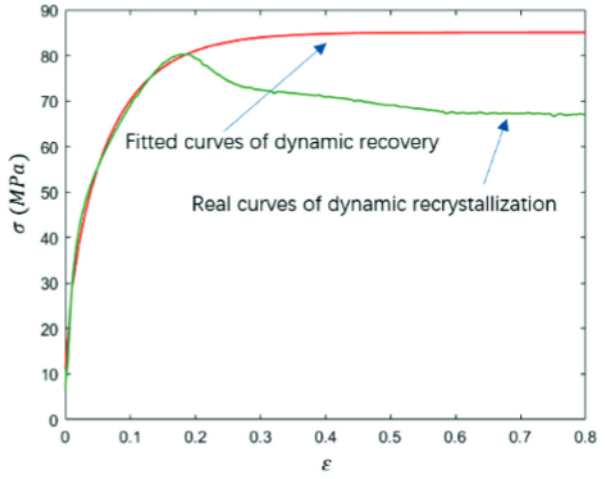

Figure 14: Dynamic recovery and dynamic recrystallization curves with a strain rate of 0.1 s^{-1} at 1273.15 K (1000 °C)

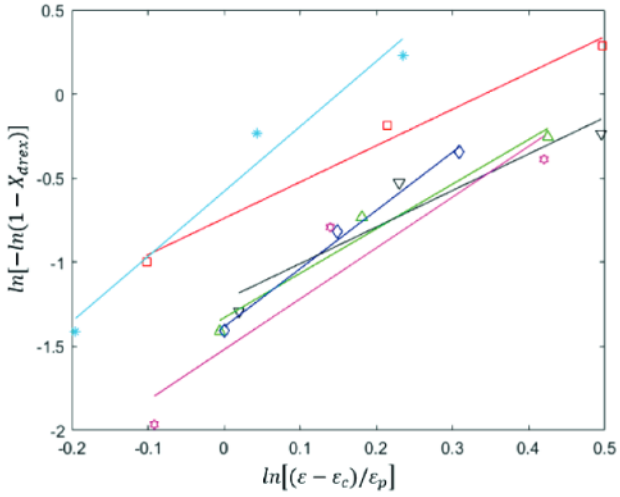

Figure 15: Relationship between $\ln[-\ln(1-X_{drex})]$ and $\ln[(\varepsilon-\varepsilon_c)/\varepsilon_p]$

where σ_{recov} is the flow stress of instantaneous dynamic recovery, σ_{drx} is the flow stress of instantaneous dynamic recrystallization, σ_s is the flow stress of steady state dynamic recovery, and σ_{ss} is the flow stress of steady-state dynamic recrystallization. The values of σ_{ss}, σ_p, σ_s and σ_c can be obtained through the relationship between θ and σ shown in Figure 12b. To obtain the values of σ_{recov} and σ_{drx}, the curves of dynamic recovery and dynamic recrystallization were drafted using the experimental data as shown in **Figure 14**. Then the values of X_{drex} could be calculated. **Figure 15** shows the relationship of $\ln[-\ln(1-X_{drex})]$ and $\ln[(\varepsilon-\varepsilon_c)/\varepsilon_p]$ that can be used to obtain the values of $\beta_d = 0.3234$ and $k_d = 2.8901$. Therefore, the kinetic model of DRX can be expressed as follows:

$$X_{drex} = 1 - \exp\left[-0.3234\left(\frac{\varepsilon - \varepsilon_c}{\varepsilon_p}\right)^{2.8901}\right] \quad (\varepsilon \geq \varepsilon_c) \quad (26)$$

4 CONCLUSIONS

1) The flow stress of LZ50 axle steel decreases with the increasing deformation temperature during hot compression. At strain rates of 0.1 s^{-1} or 1.0 s^{-1}, the peak value of the flow stress increases by approximately 30 MPa with a decrease in the temperature from 1000 °C to 900 °C, while with a decrease from 1100 °C to 1000 °C, the increase in the peak value is approximately 25 MPa. However, at a strain rate of 10.0 s^{-1}, the peak value of the flow stress increases by approximately 40 MPa with the decrease in the temperature from 1000 °C to 900 °C, which is larger than the value of 18 MPa obtained with the decrease from 1100 °C to 1000 °C.

2) The flow stress of LZ50 axle steel increases with the increasing strain rate. At deformation temperatures of 900 °C or 1000 °C, the peak value of the flow stress increases by approximately 37 MPa with the strain rate in-

creasing from 0.1 s^{-1} to 1.0 s^{-1}, while with the increase from 1.0 s^{-1} to 10.0 s^{-1}, its increase is approximately 21 MPa. However, at 1100 °C, the peak value of the flow stress increases by approximately 27 MPa with the increase from 0.1 s^{-1} to 1.0 s^{-1}, which is almost equal to 28 MPa obtained with the increase from 1.0 s^{-1} to 10.0 s^{-1}.

3) With the increase in the strain from 0.2 to 1.0, the instability area under the low deformation temperature expands due to a higher strain rate. Meanwhile, the instability area under the high deformation temperature decreases because of its softening effect. At a true strain of 0.2, the strain rate should be kept between 0.1 s^{-1} and 0.15 s^{-1} with an increase from 940 °C to 1100 °C; at a true strain of 0.6, the strain rate can be increased to 0.25 s^{-1} with the increase from 940 °C to 1100 °C; at a true strain of 1.0, the strain rate can reach 3.1 s^{-1} at 1100 °C.

4) The activation energy of dynamic recrystallization is 334.537 kJ/mol. The flow-stress constitutive equation is $\dot{\varepsilon} = 4.9079 \times 10^{10} [\sinh(0.0287699\sigma)]^{2.8923} \exp(-334537/8.3145T)$. The kinetic model of DRX $X_{drex} = 1-\exp[-0.3234((\varepsilon-\varepsilon_c)/\varepsilon_p)^{2.8901}]$ ($\varepsilon = \varepsilon_c$).

Acknowledgments

This work is supported by the National Key Research and Development Projects (No. 2018YFB1307900), Shanghai Natural Fund Project (No. 20ZR1422100) and Shanghai Talent Development Fund (No. 2019022).

5 REFERENCES

[1] Y. C. Lin, M. Chen, J. Zhong, Microstructural evolution in 42CrMo steel during compression at elevated temperatures, Mater. Lett., 62 (**2008**) 14, 2132–2135, doi:10.1016/j.matlet.2007.11.032

[2] J. Lin, Y. Liu, D. C. J. Farrugia, M. Zhou, Development of dislocation-based unified material model for simulating microstructure evolution in multipass hot rolling, Philos. Mag., 85 (**2005**) 18, 1967–1987, doi:10.1080/14786430412331305285

[3] D. Shiwen, C. Shuangmei, Hot deformation behavior and processing maps of LZ50 steel, Transactions of Materials and Heat Treatment, 37 (**2016**) 03, 223–229, doi:10.13289/j.issn.1009-6264.2016.03.038

[4] H. Zhong, Y. Wei-Wei, Rotating Bending Fatigue Property of LZ50 Steel Axle, Materials for Mechanical Engineering, 36 (**2012**) 1, 94–96, doi:10.3390/ma13020294

[5] B. Yang, Y. Zhao, Influence of Surface Rolling Time on Short Fatigue Crack Behavior of LZ50 Axle Steel, 13th International Conference on Fracture, Beijing, China, doi:10.3724/SP.J.1037.2012. 00169

[6] Y. Huo, B. Wang, J. Lin, Q. Bai, H. Ji, X. Tang, Hot compression deformation behavior and microstructure evolution rule of a high-speed railway axle steel, Indian J. Eng. Mater. S., 24 (**2017**) 6, 447–454, doi:10.3390/ma14102478

[7] Z. Jin-Wen, W. Wen-Xian, G. Jianbing, C. Sheng-Wei, W. Yu-Tian, W. Zhi-Xiang, Z. Zhi-Gang, Hot deformation behavior and hot processing map of high speed axle steel DZ2, Transactions of Materials and Heat Treatment, 41 (2020) 10, 123–129 (**2020**), doi:10.13289/j.issn.1009-6264.2020-0174

[8] S. Du, S. Chen, J. Song, Y. Li, Hot Deformation Behavior and Dynamic Recrystallization of Medium Carbon LZ50 Steel, Metall. Mater. Trans. A, 48A (**2017**) 3, 1310–1320, doi:10.1007/s111661-016-3938-0

[9] Z. Xiaohua, B. Yongqing, J. Xiaobin, Hot deformation behavior and high temperature plastic constitutive equation of LZ50 steel for axle, Heat Treatment of Metals, 45 (**2020**) 10, 31–34, doi:10.13251/j.issn.0254-6051.2020.10.006

[10] C. Zener, J. H. Hollomon, Effect of Strain Rate Upon Plastic Flow of Steel, J. Appl. Phys., 15 (**1944**) 1, 22–32, doi:10.1063/1.1707363

[11] L. Backe, Modeling the Microstructural Evolution during Hot Deformation of Microalloyed Steels, Royal Institute of Technology, Stockholm 2009, 47, doi:10.13140/RG.2.2.12251.05929

[12] H. Youlin, W. Jianbo, L. Xueshi, Z. Xiyan, L. Baifeng, L. Qing, H. Guangjie, Research Development of Hot Processing Map Theory, Materials Reports, 22 (**2008**) S3, 173–176, 10.3969/j.issn.0258-7076.2007.z1.013

[13] R. Raj, Development of a Processing Map for Use in Warm-Forming and Hot-Forming Processes, Metallurgical Transactions A, 12 (**1981**) 6, 1089–1097, doi:10.1007/BF02643490

[14] Y. V. R. K. Prasad, H. L. Gegel, J. C. Malas, J. T. Morgan, K. A. Lark, S. M. Doraivelu, D. R. Barker, Modeling of dynamic material behavior in hot deformation: Forging of Ti-6242, Metallurgical Transactions A, Physical Metallurgy and Materials Science, 15 (**1984**) 10, 1883–1892, doi:10.1007/BF02664902

[15] C. M. Sellars, W. J. Mctegart, Study on the mechanism of hot deformation, Acta Metallurgica, 14 (**1966**) 9, 1136–1140, doi:10.1016/0001-6160(66)90207-0

[16] C. M. Sellars, Modeling microstructural development during hot rolling, Material Science and Technology, 6 (**1990**) 11, 1072–1081, doi:10.1179/mst.1990.6.11.1072

[17] Y. Lin, M. Chen, Numerical simulation and experimental verification of microstructure evolution in a three-dimensional hot upsetting process, J. Mater. Process. Tech, 209 (**2009**) 9, 4578–4583, doi:10.1016/j.jmatprotec.2008.10.036

[18] F. Wei, X. Fujia, Microstructure evolution and dynamic recrystallization model of 20CrMnTiH steel during hot compression, Journal of Plasticity Engineering, 21 (**2014**) 3, 78–84, doi:10.3969/j.issn.1007-2012.2014.03.016

[19] Y. Xingsheng, W. Chuan, S. Ruxing, W. Yuchanag, W. Zhe, Microstructure evolution of 55NiCrMoV7 die steel during forging processing: Experiment and simulation, Journal of Plasticity Engineering, 28 (**2021**) 6, 174–184, doi:10. 3969/j.issn.1007-2012.2021.06.023